# PHOTOCHEMISTRY AND VERTICAL MIXING

S. K. ATREYA
*The University of Michigan*

B. R. SANDEL
*The University of Arizona*

and

P. N. ROMANI
*Science Systems and Applications, Inc.*

*The only known photochemically active volatile in the atmosphere of Uranus is methane. Other species normally present as gases in the atmospheres of Jupiter and Saturn are simply not likely to be gaseous in the photolytic regime of the upper troposphere and the stratosphere of Uranus due to the low tropopause temperature. The photolysis of methane produces primarily ethylene, ethane and acetylene. The latter two species condense near the tropopause. In addition, formation and subsequent condensation of polyacetylenes is likely near the 0.1 mbar level. Transport of the hydrocarbon ices to the deeper troposphere, followed by evaporation or pyrolysis and high-pressure chemistry and subsequent convection appears to be responsible for the stability of methane in the upper atmosphere. The vertical mixing on Uranus, as characterized by the eddy diffusion coefficient, is sluggish, with a typical equatorial value at the homopause of 10,000 $cm^2\ s^{-1}$. It is perhaps related to the virtual lack of internal energy, coupled with a low input of solar as well as magnetospheric energy. Jupiter and Saturn, which have internal energy sources approximately equivalent to the absorbed solar energy, have eddy mixing coefficients 2 and 3 to 4 orders of magnitude greater, respectively, than that on Uranus. This chapter discusses theory, observations, and their interpretation in terms of the relevant photochemistry and atmospheric mixing on Uranus.*

The atmosphere of Uranus differs from those of the other giant planets many respects. It is the only planet in the outer solar system that lacks a bstantial internal energy source. One possible consequence of a meager ernal energy source is sluggish vertical mixing in the homosphere. Al-ɔugh the Voyager ultraviolet solar occultations returned the first conclusive idence, weak mixing in the upper atmosphere of Uranus had been specu-ed for some time on the basis of IUE (International Ultraviolet Explorer) servations of acetylene, and the structure in the temperature profile mea-red from groundbased visible stellar occultation observations.

Photochemistry on both Uranus and Neptune is limited to a single parent nstituent, methane ($CH_4$). Although other photochemically active par-ts—ammonia, water, hydrogen sulfide—are removed by condensation in ɛ deep troposphere, substantial amounts of methane remain in vapor phase en above the tropopause cold-trap (the methane ice cloud forms at a pres-re level of approximately 1200 to 1500 mbar). Photolysis of methane re-lts in the formation of stable gas-phase hydrocarbons such as ethane $_2H_6$), acetylene ($C_2H_2$), ethylene ($C_2H_4$), and polymers of acetylenes (po-ynes), which are loosely referred to as polyacetylenes ($C_{2n}H_2$, $n$ = 2,3,4 .). With the exception of $C_2H_4$, whose abundance is low, all other photo-emical products of $CH_4$ will condense, mostly in the lower stratosphere. ɜ on Jupiter and Saturn, however, the atmospheric abundance of $CH_4$ re-ains stable. This is the consequence of snow-out or rain-out of the conden-tes followed by re-evaporation, pyrolysis and/or synthesis in the deep trop-phere where the temperatures are warmer. In this chapter pre-Voyager, i.e., ırth-based observations relevant to the question of photochemistry and ver-ɜal mixing are discussed first (Sec. I). In Sec II Voyager observations, pri-arily the ultraviolet occultations and their analysis, are presented. Photo-ıemical interpretation of the observations is discussed in Sec. III from the ewpoint of gas-phase and condensed hydrocarbons, and in Sec. IV in terms the atmospheric mixing. The final section summarizes current understand-g of the problem and presents some directions for future studies.

## I. PRE-VOYAGER OBSERVATIONS

Previous to the Voyager encounter of Uranus, Earth-based observations, om both the ground and the IUE satellite, provided information about the ɔmposition, thermal structure and the aerosol content of the planet's upper mosphere. Relevant observations are reviewed here briefly; an extensive view of pre-Voyager knowledge of Uranus can be found in Bergstralh 984).

Information about the gaseous composition of Uranus' stratosphere ıme from analysis of observations in the infrared and ultraviolet. The in-ared spectrum of Uranus was notable for the absence of emission features methane and ethane, while the same features were seen in the spectrum of

Neptune (Macy and Sinton 1977; Gillet and Rieke 1977; Orton et al. 1983). Only upper limits could be placed on the abundances of $CH_4$ and $C_2H_6$. The limit on the methane abundance, $3 \times 10^{-5}$ (Orton et al. 1983), was in accord with the amount expected from saturation at the tropopause, and was lower than the value on any other outer planet. The upper limit on ethane was also low, $3 \times 10^{-8}$ (Orton et al. 1983). Caldwell et al. (1984) and Encrenaz et al. (1986) detected $C_2H_2$ from analysis of IUE spectra; the analysis of Encrenaz et al. yielded a $C_2H_2$ column abundance of $(3.4 \pm 1.7) \times 10^{16}$ cm$^{-2}$. From this analysis of their $C_2H_2$ data, Encrenaz et al. estimated a low value of the eddy mixing coefficient in the stratosphere, on the order of $10^5$ cm$^2$ s$^{-1}$ at the methane homopause. With the inclusion of $H_2$ Rayleigh scattering, which was not considered by Encrenaz et al., the eddy diffusion coefficient implied by the $C_2H_2$ data would be even smaller, around $10^4$ cm$^2$s$^{-1}$. There were also indications of a factor of 3 decrease in the $C_2H_2$ abundance with time/planetary latitude. Besides the above-mentioned hydrocarbons, there was speculation about the helium abundance on Uranus by Orton (1986). From analysis of the infrared spectra, Orton proposed a 40% volume mixing ratio for helium. However, this conclusion turned out to be erroneous, as it was based upon a model that excluded the effects of a possible stratospheric aerosol layer because such a layer seemed too *ad hoc*.

Observations in the infrared (Tokunaga et al. 1983; Orton et al. 1983) and stellar occultations in the visible (Dunham et al. 1980; French et al. 1983) produced data on the thermal structure. The infrared observations are sensitive to the 100-mbar region, where it was determined that Uranus has a broad temperature minimum on the order of 50 K. Analysis of the stellar occultations yielded a mean temperature of the upper stratosphere (0.3 to 30 μbar) in the range of 90 to 160 K. These temperatures are in reasonably good accord with the Voyager 2 observations. Interpreting the small-scale features recorded in the temperature profiles in terms of upward propagating gravity waves, French et al. concluded that the eddy diffusion coefficient in the upper atmosphere (0.3 to 30 μbar) must be $< 3 \times 10^4$ cm$^2$ s$^{-1}$ to permit vertical propagation of these waves.

Attempts to determine the presence and properties of aerosols in the stratosphere were made from analysis of the geometric albedo of Uranus from the ultraviolet to the near infrared. From the ultraviolet observations, it was uncertain whether aerosols were even present in the upper atmosphere. Based upon an examination of the solar reflection spectrum of Uranus in the ultraviolet, Savage et al. (1980) argued for the presence of aerosols in the upper atmosphere, while later Caldwell et al. (1981) argued against it. The source of disagreement was the choice of a proper solar analog star. A detailed analysis of the Uranus spectrum from the ultraviolet to the near infrared by Baines and Bergstralh (1986) required a haze layer above the methane ice cloud in the upper troposphere, but it was uncertain whether the haze extended into the stratosphere. Modeling of $CH_4$ photochemistry by Atreya and Ponthieu

(1983) and Romani (1986) showed that condensation of $C_2H_2$ and $C_2H_6$ to their respective ices was a probable source of aerosols in the lower stratosphere.

In summary, prior to the Voyager 2 encounter, only the following fragmentary information was available about the Uranus stratosphere—the atmospheric region where most of the photochemical activity occurs. The abundance of methane and its photolysis products were the lowest of any outer planet and there were indications that the eddy mixing coefficient was also the lowest. The thermal structure below 1 mbar was fairly well constrained. It was possible that aerosols were present in the lower stratosphere, and their likely source was the condensation of the hydrocarbon by-products of methane photochemistry.

## II. VOYAGER OBSERVATIONS AND ANALYSIS

### A. Voyager Ultraviolet Occultation

Ultraviolet Spectrometer (UVS) observations of the occultations of the Sun and the star $\gamma$ Pegasi by the atmosphere of Uranus have revealed its composition and temperature structure. This investigation was discussed in detail by Herbert et al. (1987). Smith and Hunten (1990) reviewed the occultation technique and a number of specific applications. Here we summarize the results at Uranus (see also the chapter by Conrath et al.).

The UVS occultation experiments measured the opacity of the atmosphere as a function of altitude and wavelength. The UVS recorded the unattenuated spectrum of the source, and then spectra modified by atmospheric absorption as the line of sight to the source moved through the atmosphere. H, $H_2$ and a variety of hydrocarbons have strong, characteristic absorption cross sections within the 500 to 1700 Å spectral range of the UVS. From the measured opacities, Herbert et al. (1987) deduced altitude profiles of $H_2$ and H, and hence the temperature profile of the atmosphere, over the pressure range of $10^{-6}$ to 500 μbar. The hydrocarbon concentrations they deduced at Uranus are lower than at similar pressure levels at Jupiter and Saturn, making the hydrocarbons more difficult to detect.

The reduced mixing ratio of hydrocarbons is advantageous in that it permits the determination of the altitude profile of $H_2$, the dominant constituent, at pressures much higher than probed on Jupiter or Saturn. Rayleigh scattering by $H_2$ contributes negligibly to opacity at column abundance $\lesssim 10^{24}$ cm$^{-2}$. At Jupiter and Saturn, the atmospheres are opaque because there is significant hydrocarbon absorption at much lower column abundances of $H_2$, so Rayleigh scattering was not detectable. In contrast, at Uranus Rayleigh scattering is an important contributor to the opacity of the atmosphere at wavelengths longward of ~ 1500 Å; analysis of the opacity profiles must take this source of opacity into account. Rayleigh scattered sunlight emerging from the at-

mosphere has been used by Yelle et al. (1989) as an additional diagnostic of hydrocarbon distributions, as we discuss in Sec. II.D.

### B. Analysis Procedures

In principle, it is possible to invert the absorption profiles mathematically to yield altitude profiles of the constituents. However, in practice, such inversions have proven sensitive to several sources of systematic error. Inversion is complicated by instrumental scattering of H Lyman $\alpha$, and by the facts that several species absorb in the same wavelength interval, that the scale height must be determined simultaneously with all the altitude profiles in a self-consistent way, and that the finite size of the Sun projected on the atmosphere of Uranus mixes absorption signatures from a range of altitudes.

As an alternative to inversion, Herbert et al. (1987) adopted the approach of comparing observed occultation profiles with synthetic profiles computed from a specific model atmosphere, the known absorption characteristics of the assumed constituents, the occultation geometry and the characteristics of the UVS response. The model atmosphere was adjusted until the absorption profiles predicted by the model were consistent with the observed profiles at each wavelength. For the H and $H_2$ altitude profiles, the model atmosphere was based on integration of the hydrostatic equation, including terms for centrifugal acceleration and the variation of gravity with altitude. The concentration of each species was fixed at a reference altitude, and the temperature was continuously interpolated between adjustable values at five altitudes.

A different technique is needed to include the effects of hydrocarbons. These species are photochemically active, so their altitude profiles cannot be predicted by the simple techniques described in the previous paragraph. Instead, Herbert et al. included in the model atmosphere the hydrocarbon profiles computed from photochemical models. After testing a range of models by comparing the computed to the observed lightcurves, the best fitting model was selected. The photochemical models are discussed in Sec. III.

### C. The Occultation Observations and Results

The ingress solar occultation probed the limb near the rotation equator. Because of constraints on scan platform pointing imposed by other observations, the egress solar occultation was not observed. The UVS probed the polar atmosphere by observing both ingress and egress occultations of $\gamma$ Pegasi. Table I gives geometrical parameters for these occultations, and Fig. 1 illustrates the geometry.

Because the hydrocarbon mixing ratios are lower at Uranus than at Jupiter and Saturn, at Uranus these species are more difficult to detect by the occultation technique. Herbert et al. (1987) cautiously identified the absorption signature of $C_2H_2$, and evidence for absorption by $C_2H_6$, but were able only to place an upper limit on $CH_4$ concentrations. Figure 2 compares an

**TABLE I**
**Occultation Geometry**

| | Sun | γ Pegasi ingress | γ Pegasi egress |
|---|---|---|---|
| ,atitude (deg) | 3.6 S | 63.7 S | 69.7 N |
| :ange to tangent point (km) | $1.7 \times 10^5$ $7.6 -$ | $1.0 \times 10^5$ | $1.0 \times 10^5$ |
| z/dt (km $s^{-1}$) | 8.2 | 17.8 | 17.8 |
| ·ample time (s) | 0.32 | 0.32 | 0.32 |

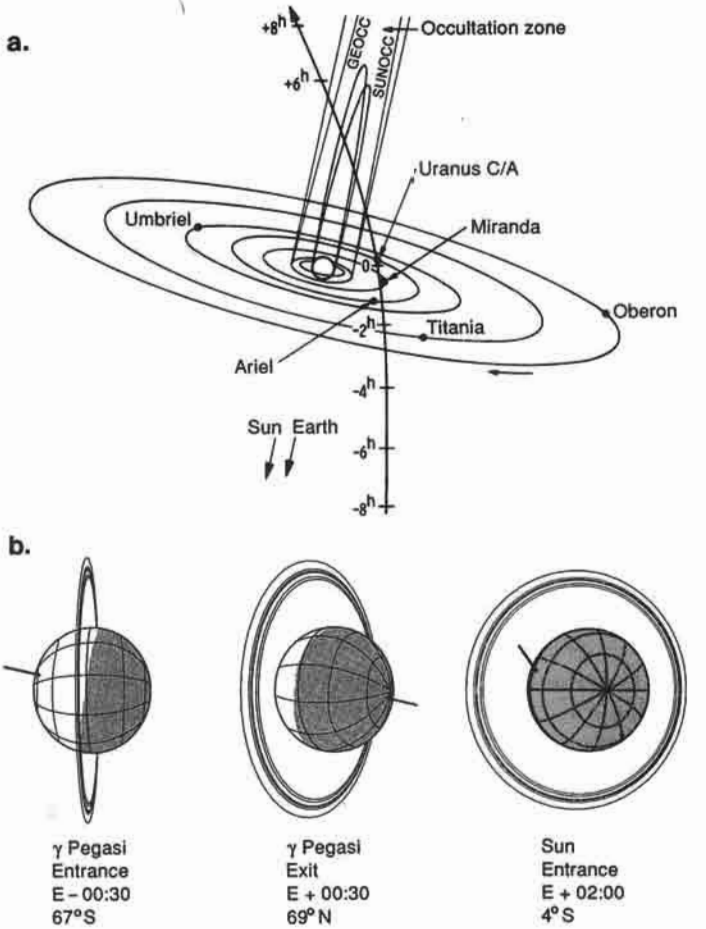


ig. 1. Occultation geometry. (a) Projection into the Voyager 2 orbit plane of the Uranian ring and satellite systems with Voyager orbit superimposed (figure from Stone and Miner 1986). (b) Line-of-sight tracks of the three occultations: solar, γ Pegasi and ν Geminorum, projected onto the plane of the sky in the vicinity of Uranus as seen from Voyager 2 (Herbert et al. 1987).

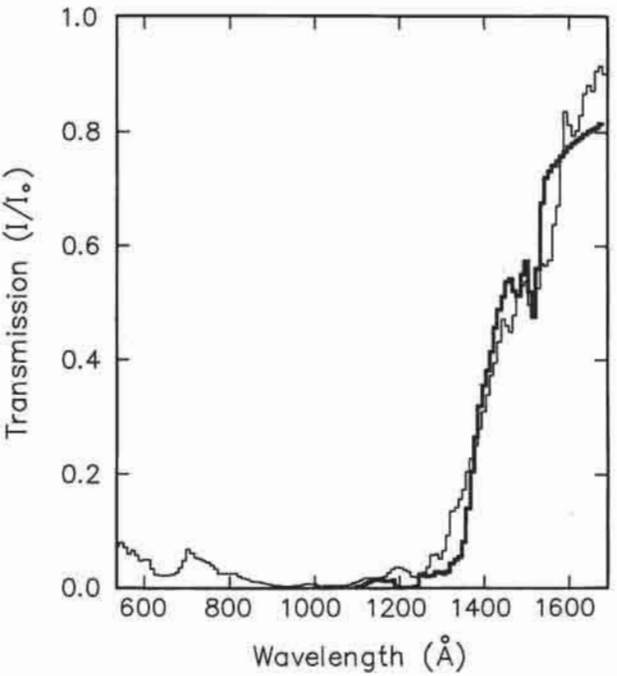


Fig. 2. Solar occultation transmission curves showing the $C_2H_2$ absorption in the Uranus atmosphere. The light line shows the observed spectrum which is an average between 295 and 375 km. The heavy line is a model used to match the data. Values below 1000 Å are spurious (Herbert et al. 1987).

observed transmission spectrum with a model spectrum computed from a model atmosphere including $C_2H_2$. The local minimum in the curve at ~ 1500 Å corresponds to a maximum in the absorption cross section of $C_2H_2$; Herbert et al. interpreted this structure as evidence for $C_2H_2$. A preponderance of the weight in this interpretation is given to the feature near 1500 Å, because at shorter wavelengths, the measured spectrum is affected more strongly by scattering inside the instrument from the solar H Lyman-α line.

Nevertheless, the observations show evidence for the $C_2H_2$ absorption feature near 1300 Å as well as the more prominent feature just discussed. Figure 3 compares the atmospheric opacity observed at a particular level with the opacities expected from Rayleigh scattering and from $C_2H_2$ absorption. The column abundances of $H_2$ and $C_2H_2$ have been adjusted so that their sum gives the best fit to the measured opacity. The downward trend from short to long wavelength in the measured opacity is well matched by Rayleigh scattering, but the data show increases above the Rayleigh scattering baseline at positions that correspond well to the peaks in opacity expected for $C_2H_2$. Taken together, we regard these plots as good evidence that $C_2H_2$ has been measured.

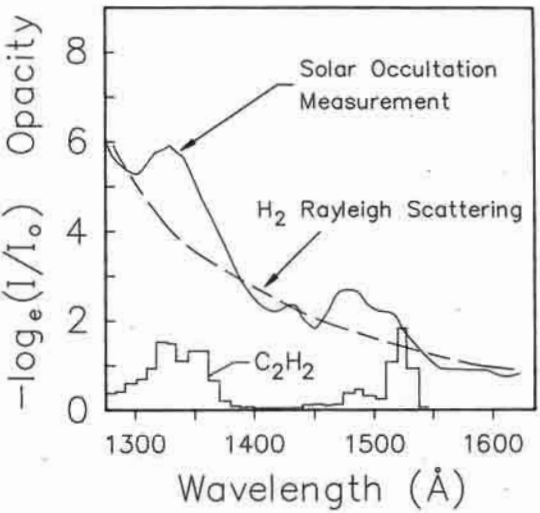


Fig. 3. Least-squares fit of model opacity to observed transmission spectrum at Uranus. Solar occultation transmission is plotted as -ln ($I/I_o$) as a function of λ. A function of the form $\sum_i \tau_i$, for $i$ = $H_2$ and $C_2H_2$ ($\tau_i = N\,\sigma_i$; $N$ is the column abundance and $\sigma_i$ is the cross section of constituent $i$ at wavelength λ) was fitted to -ln ($I/I_o$). Individual $\tau_i$'s are plotted separately. Match of the $C_2H_2$ profile as well as of the $H_2$ Rayleigh scattering shape of the observed $I/I_o$ are apparent (Herbert et al. 1987).

To estimate the mixing ratio of $C_2H_2$, information about its altitude distribution is needed. Elsewhere we use distributions estimated from considerations of photochemistry and vertical mixing, but it is desirable to derive a more model-independent value as well. Herbert et al. assumed complete mixing in the altitude range over which $C_2H_2$ was detected, so the $C_2H_2$ concentration follows the scale height of the background gas, about 50 km. Under this assumption, they derived a $C_2H_2$ mixing ratio of $\sim 1 \times 10^{-8}$. This estimate applies over the range of 200 to 400 km. At the bottom of this range, the $H_2$ partial pressure is 0.81 mbar and its concentration is $7 \times 10^{16}$ cm$^{-3}$. Observations of Uranus at 7 to 14 μm using the Infrared Telescope Facility (IRTF) place a maximum mixing ratio of $9 \times 10^{-9}$ on the stratospheric $C_2H_2$ (Orton et al. 1987). The IUE observations below 2000 Å yield a mixing ratio of $1 \times 10^{-8}$ for $C_2H_2$ (Caldwell et al. 1988) in agreement with the Voyager UVS results, and essentially in agreement with the pre-Voyager observations of Encrenaz et al. (1986).

The transmission spectra also show evidence for $C_2H_6$, but the relatively featureless cross section of this species (compared to that of $C_2H_2$) makes its identification more difficult. Its presence is inferred from the shape of the observed transmission spectrum in the 1350 to 1450 Å region. Here the agreement of model and measured transmission spectra is improved by inclusion of $C_2H_6$ at a mixing ratio of several times $10^{-8}$, estimated in the same

manner as described in the previous paragraph for $C_2H_2$. The IRTF measurements by Orton et al. (1987*b*), mentioned above, impose an upper limit of $2 \times 10^{-8}$ on the stratospheric $C_2H_6$ mixing ratio.

Herbert et al. were able to establish only an upper limit to the $CH_4$ concentration because its mixing ratio is low and because the detection window longward of the $H_2$-band absorption and shortward of the long-wavelength cutoff in $CH_4$ absorption is strongly affected by instrumental scattering of the solar H Lyman-α line. Uncertainty in correcting for this scattering reduces the confidence of determinations based on this region of the spectrum. The upper limit on the $CH_4$ mixing ratio is about $10^{-7}$, and it applies over roughly a 100 to 1 μbar pressure range (300–500 km). As in the case of the other hydrocarbons, this estimate is based on the assumption of complete mixing in the altitude range.

The occultation of γ Pegasi showed that the temperature structure of the atmosphere in the vicinity of the rotation poles does not differ markedly from that near the equator. The intrinsic altitude resolution of a point source, combined with the fact that the UVS always operated within its linear signal range, partially offset the lower signal-to-noise ratio resulting from the faintness of the source. The derived atmospheric profiles are consistent with those for the equatorial region, except for a possible offset in altitude scales of approximately 70 km. Nevertheless, because of the lower signal-to-noise ratio at long wavelengths, the hydrocarbon profiles are rather poorly constrained by the stellar occultation. Variations of the order suggested later to account for the apparent equator-to-pole differences in hydrocarbon mixing ratios are not ruled out by these observations. The atmospheric composition and density profiles as obtained from the occultation experiment are summarized in Fig. 4.

### D. Far-Ultraviolet Reflectance Spectrum

The far-ultraviolet spectrum of sunlight reflected from Uranus contains information on the distribution of hydrocarbons in the upper atmosphere. Uranus differs in this respect from Jupiter and Saturn, where hydrocarbon mixing ratios are great enough to absorb sunlight high in the atmosphere, so that little is reflected. The lower hydrocarbon mixing ratios at Uranus permit the solar far ultraviolet to penetrate to pressure levels near 1 mbar, where Rayleigh and Raman scattering by $H_2$ are important. Some hydrocarbons are present at this pressure level, and they impose their absorption signature on the spectrum of the reflected sunlight.

Yelle et al. (1987*a*) applied these considerations to analyze a Voyager UVS reflectance spectrum taken near the subsolar point of Uranus (and hence near the rotation pole). Using the measured intensity of the Raman-shifted solar H Lyman-α line at 1280 Å, they constrained the $CH_4$ column abundance at altitudes above ~0.5 mbar to be $< 5 \times 10^{16}$ cm$^{-2}$. To account for this low

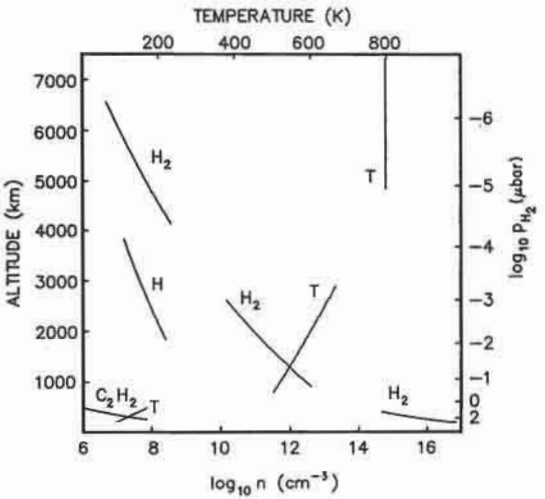


Fig. 4. The ultraviolet occultation results at Uranus: altitude profiles of the densities of $H_2$, H and $C_2H_2$, and of the atmospheric temperature. Altitudes are referenced from the 1-bar level located at an equatorial radius of 25,550 km. The right-hand ordinate shows the corresponding pressure in μbar (Herbert et al. 1987).

column abundance, they invoked weak vertical mixing, characterized by $K \approx 200\ cm^2s^{-1}$, between 0.5 and 100 mbar.

A more extensive analysis along the same lines has been carried out by Yelle et al. (1989), who interpreted UVS observations of the solar reflection spectrum in the 1250 to 1700 Å range. They computed $CH_4$ and $C_2H_2$ absorption by means of a three-layer model of the atmosphere that was constrained by knowledge of the stratosphere and the temperature structure of the upper atmosphere. An example of their results is shown in Fig. 5. The sharp change in albedo between 1500 and 1550 Å is diagnostic of $C_2H_2$ absorption, and fitting the amplitude of this change defines the $C_2H_2$ abundance in the model. Sensitivity to the $CH_4$ abundance is confined mainly to the wavelength region below 1350 Å. Generally speaking, Yelle et al. found that the hydrocarbon mixing ratios in the layers of their model atmosphere affect the albedo in different spectral regions, leading to a well-determined fitting procedure. The mixing ratios inferred for the region above 3 mbar were $(1 - 3) \times 10^{-7}$ for $CH_4$ and $(0.6 - 1.2) \times 10^{-8}$ for $C_2H_2$.

This is a substantially lower mixing ratio of $CH_4$ than expected on the basis of the photochemical models that give a good match to the absorption profiles measured in the occultation experiment. A possible resolution of this apparent discrepancy may lie in the fact that only $C_2H_2$ is definitely measured in the solar occultation. If K is large enough that $C_2H_2$ is fully mixed as high as the 500 μbar level, then the optical depth at H Lyman-α due to $C_2H_2$

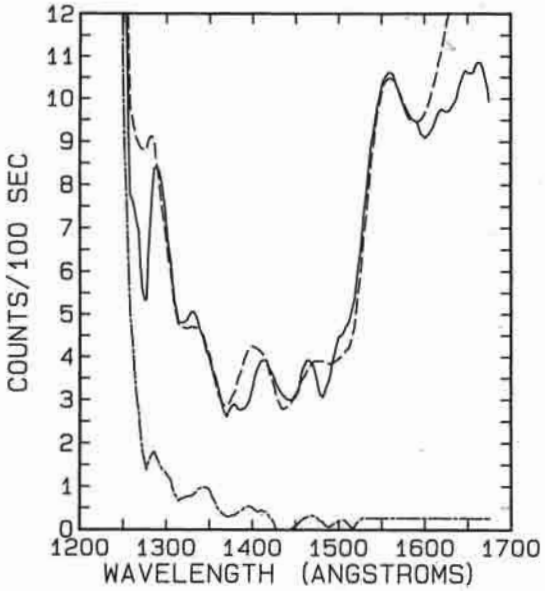


Fig. 5. Comparison of a model (dashed line) with the observed (solid line) far-ultraviolet reflectance spectrum from the subsolar region of Uranus. The dot-dash line represents the effect of $H_2$ emissions that have been removed from the data. The structure in the albedo is due mainly to $C_2H_2$ absorption, with a significant contribution from $CH_4$ (Yelle et al. 1989).

absorption will be small (Herbert et al. 1987). Then, postulating a $CH_4$ column abundance lower than predicted (but consistent with observations) can force consistency between the occultation and solar reflection measurements.

Although this explanation cannot be ruled out *a priori*, we prefer an alternate hypothesis, suggested by Herbert et al. (1987), that does not demand abandoning the results of the photochemical models and that the observations support. This alternate view involves variations in the hydrocarbon abundance from the equator (where the solar occultation was observed) to the rotation pole (where analysis of the reflected spectrum applies).

Yelle et al. (1989) report variations in the far-ultraviolet albedo across the disk of Uranus that are consistent with diminished abundances of hydrocarbons at the rotation pole. Unfortunately, the signal-to-noise ratio of spectra taken near the equator is too low to determine the hydrocarbon mixing ratios reliably as needed for detailed comparison with the occultation data. Nevertheless, we have good evidence that latitudinal variations could account for much of the difference between the hydrocarbon abundances inferred from the solar occultation and those inferred from the albedo. This is probably only a part of the complete explanation; Yelle et al. (1989) discussed details suggesting that other factors are also important.

## III. METHANE PHOTOCHEMISTRY AND HAZE PRODUCTION

### A. Introduction: Chemistry and Condensation

Aeronomical interpretation of the observed distributions of the neutrals in the Uranian atmosphere requires an understanding of the middle atmospheric photochemical processes. The stratosphere of Uranus is much simpler photochemically than that of either Jupiter or Saturn. On Uranus, the only photochemically active trace species is $CH_4$. Other possible active species, $H_2S$, $NH_3$ and $PH_3$ are removed from the vapor phase by condensation into various clouds well below the tropopause (Atreya and Romani 1985; Fegley and Prinn 1986; de Pater et al. 1989). Below the tropopause, photolysis is not appreciable because Rayleigh scattering by $H_2$ limits the penetration of ultraviolet photons capable of initiating photolysis.

The photochemistry of methane has been studied extensively for Jupiter (Strobel 1969,1973,1975; Atreya et al. 1981; Gladstone 1982) and Saturn (Waite 1981; Atreya 1982; Atreya et al. 1984). These models are very similar, one-dimensional methane photochemistry models that carry through the chemistry to $C_2$ hydrocarbons produced by methane photolysis. For Titan studies, Yung et al. (1984) added on the photochemistry of the polyynes.

The Jupiter and Saturn models are equally applicable to Uranus as the photochemistry is similar—the photolysis of a trace amount of methane by solar ultraviolet in a background $H_2$-He atmosphere. The notable differences for Uranus are that, due to the low temperatures and methane mixing ratio in the stratosphere, there is a large production of the polyynes, and a strong condensation sink for acetylene, ethane and the polyynes due to condensation to the ice phase at pressures $\gtrsim 0.05$ mbar. Thus, photochemical models for Uranus need to include both the polyyne photochemistry and a condensation sink. The models of Romani and Atreya (1989) and Summers and Strobel (1989) include both processes and are similar photochemically. The pre-Voyager model of Atreya and Ponthieu (1983) was the first to incorporate condensation of acetylene and ethane in Uranus' atmosphere. Before proceeding with the details of methane photochemistry on Uranus, we review the relevant photochemical and condensation processes.

A schematic of the photochemical pathways used in the Romani and Atreya model (1988,1989) is shown in Figs. 6 and 7. The photolysis reactions and quantum yields are listed in Table II, and the chemical kinetic reaction rate coefficients are listed in Table III. The species in the model include: methane ($CH_4$), the nonequilibrium $C_2$ hydrocarbons: ethylene ($C_2H_4$), acetylene ($C_2H_2$) and ethane ($C_2H_6$), and a plethora of radicals: methyl ($CH_3$), methylidyne (CH), ground-state methylene ($^3CH_2$), excited methylene ($^1CH_2$), ethynyl ($C_2H$), vinyl ($C_2H_3$) and ethyl ($C_2H_5$), and atomic hydrogen (H).

The photolysis of methane, which initiates the chemistry, is primarily

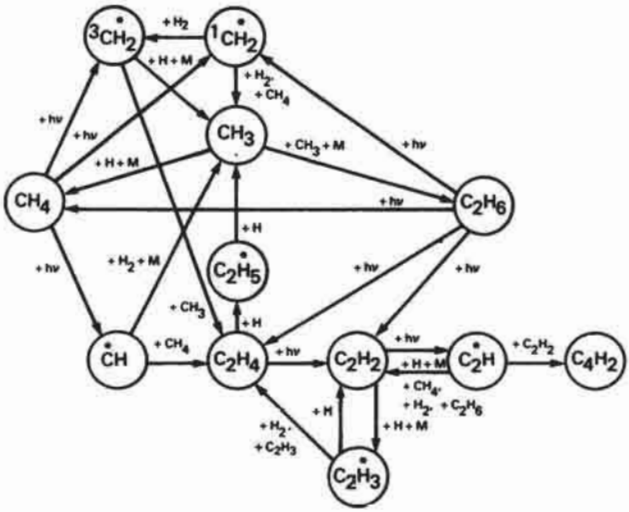


Fig. 6. Reaction pathways for methane photochemistry. A (*) denotes a radical assumed to be in local photochemical equilibrium. Figure is adapted from Atreya and Romani (1985), with the exception of right-most pathways producing $C_4H_2$.

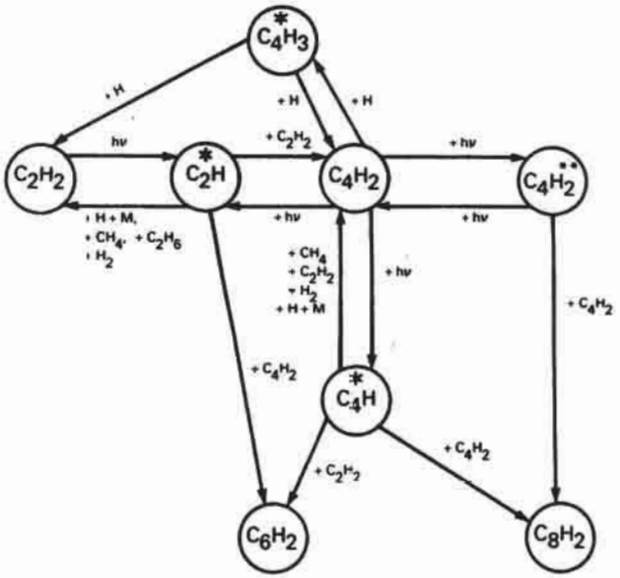


Fig. 7. Reaction pathways for diacetylene photolysis. A (*) denotes a radical assumed to be in local photochemical equilibrium, and (**) denotes a metastable-excited species (figure adapted from Romani and Atreya 1988).

| Process | | | | Quantum Efficiency[1] | | | Reference |
|---|---|---|---|---|---|---|---|
| | | | | Ly α | elsewhere | | |
| J1a | $CH_4 + h\nu$ | → | $^3CH_2 + 2H$ | 0.51 | 0.0 | | 2 |
| J1b | | → | $^1CH_2 + H_2$ | 0.41 | 1.0 | | |
| J1c | | → | $CH + H + H_2$ | 0.08 | 0.0 | | |
| J2a | $C_2H_2 + h\nu$ | → | $C_2H + H$ | λ<1500Å—0.40<br>λ>1500Å—0.18 | | | 3 |
| | | | | Ly α | elsewhere | | |
| J3a | $C_2H_4 + h\nu$ | → | $C_2H_2 + H_2$ | 0.51 | 0.51 | | 1 |
| J3b | | → | $C_2H_2 + 2H$ | 0.49 | 0.49 | | |
| | | | | Ly α | elsewhere | | |
| J4a | $C_2H_6 + h\nu$ | → | $C_2H_2 + 2H_2$ | 0.25 | 0.27 | | 1, 4 |
| J4b | | → | $C_2H_4 + 2H$ | 0.30 | 0.14 | | |
| J4c | | → | $CH_4 + {}^1CH_2$ | 0.25 | 0.02 | | |
| J4d | | → | $C_2H_4 + H_2$ | 0.13 | 0.56 | | |
| J4e | | → | $2\,C\,H_3$ | 0.08 | 0.01 | | |
| | | | | λ<1650Å | 1650–2050Å | >2050Å | |
| J5a | $C_4H_2 + h\nu$ | → | $C_4H + H$ | 0.2 | 0.0 | 0.0 | 5 |
| J5b | | → | $C_2H_2 + C_2$ | 0.1 | 0.06 | 0.0 | |
| J5c | | → | $2C_2H$ | 0.03 | 0.01 | 0.0 | |
| J5d | | → | $C_4H_2$** | 0.67 | 0.93 | 1.0 | |

[1] Gladstone (1982).
[2] Watanabe et al. (1953); McNesby and Okabe (1964); Calvert and Pitts (1966); Gorden and Ausloos (1967); Mount et al. (1977); Slanger (1982).
[3] Nakayama and Watanabe (1964); Okabe (1981); Laufer (1982).
[4] Lias et al. (1970).
[5] Glicker and Okabe (1987). In the model it is assumed that all of the $C_2$ is quickly converted to $C_2H_2$ in the following manner (Pasternack and McDonald 1979) $C_2 + H_2 \rightarrow C_2H + H$ followed by R16–R19 (see Table III).

**TABLE III**
**Methane Photochemistry**

| Reactions | | | Reaction Rate | References |
|---|---|---|---|---|
| R1 | $^1CH_2 + H_2$ | $\rightarrow CH_3 + H$ | $7.0 \times 10^{-12}$ | Laufer 1981*a* |
| R2 | $^1CH_2 + CH_4$ | $\rightarrow CH_3 + CH_3$ | $1.9 \times 10^{-12}$ | Laufer 1981*a* |
| R3 | $CH + CH_4$ | $\rightarrow C_2H_4 + H$ | $1.0 \times 10^{-10}$ | Butler et al. 1981 |
| R4 | $CH + H_2 + M$ | $\rightarrow CH_3 + M$ | $3.1 \times 10^{-30} \exp(457/T)$ | Butler et al. 1981 |
| R5 | $H + CH_3 + M$ | $\rightarrow CH_4 + M$ | $3.1 \times 10^{-29} \exp(457/T)$ | Troe 1977; Patrick et al. 1980 |
| R6 | $CH_3 + CH_3 + M$ | $\rightarrow C_2H_6 + M$ | $1.0 \times 10^{-26} \exp(506/T)$ | Callear and Metcalfe 1976; Vandenbergh 1976 |
| R7 | $H + H + M$ | $\rightarrow H_2 + M$ | $2.5 \times 10^{-31} T^{-0.6}$ | Ham et al. 1970 |
| R8 | $H + C_2H_2 + M$ | $\rightarrow C_2H_3 + M$ | $6.4 \times 10^{-25} T^{-2} \exp(-1200/T)$ | Payne and Steif 1976 |
| R9 | $H + C_2H_3$ | $\rightarrow C_2H_2 + H_2$ | $1.5 \times 10^{-11}$ | Keil et al. 1976 |
| R10 | $H_2 + C_2H_3$ | $\rightarrow C_2H_4 + H$ | $3.0 \times 10^{-13} \exp(-5570/T)$ | Yung and Strobel 1980 |
| R11 | $H + C_2H_4 + M$ | $\rightarrow C_2H_5 + M$ | $1.1 \times 10^{-23} T^{-2} \exp(-1040/T)$ | Michael et al. 1973; Lee et al. 1978 |
| R12 | $H + C_2H_5$ | $\rightarrow CH_3 + CH_3$ | $1.9 \times 10^{-10} \exp(-440/T)$ | Halstead et al. 1970 |
| R13 | $^3CH_2 + H + M$ | $\rightarrow CH_3 + M$ | $3.1 \times 10^{-30} \exp(457/T)$ | Gladstone 1982 |
| R14 | $CH_3 + {}^3CH_2$ | $\rightarrow C_2H_4 + H$ | $7.0 \times 10^{-11}$ | Pilling and Robertson (1975); Laufer and Bass 1975 |
| R15 | $^3CH_2 + C_2H_2 + M$ | $\rightarrow CH_3C_2H + H$ | $4.0 \times 10^{-26} \exp(634/T)$<br>$k_\infty = 2.2 \times 10^{-12}$ | Terao et al. 1963; Laufer 1981*a*; Yung et al. 1984 |
| R17 | $C_2H + H_2$ | $\rightarrow C_2H_2 + H$ | $5.7 \times 10^{-11} \exp(-1762/T)$ | Laufer 1982; Brown and Laufer 1981 |
| R18 | $C_2H + CH_4$ | $\rightarrow C_2H_2 + CH_3$ | $6.5 \times 10^{-12} \exp(-503/T)$ | Laufer 1981*b*, 1982 |
| R19 | $C_2H + C_2H_6$ | $\rightarrow C_2H_2 + C_2H_5$ | $1.8 \times 10^{-11} \exp(-302/T)$ | Laufer 1981*b*, 1982 |
| R20 | $C_2H + C_2H_2$ | $\rightarrow C_4H_2 + H$ | $5.0 \times 10^{-11}$ | Okabe 1981 |
| R21 | $CH_3C_2H + H$ | $\rightarrow CH_3 + C_2H_2$ | $9.7 \times 10^{-12} \exp(-1550/T)$ | von Wagner and Zellner 1972 |
| R22 | $^1CH_2 + H_2$ | $\rightarrow {}^3CH_2 + H_2$ | $1.0 \times 10^{-12}$ | Laufer 1981*a* |
| R23 | $C_2H_3 + C_2H_3$ | $\rightarrow C_2H_4 + C_2H_2$ | $5.3 \times 10^{-12}$ | McFadden and Currie 1973 |
| R24 | $C_2H_2 + H$ | $\rightarrow C_2H_3$ | $1.39 \times 10^{-10} \exp(-1184/T)$ | Nava et al. 1986 |
| R25a | $C_4H_3 + H$ | $\rightarrow C_4H_2 + H_2$ | $1.2 \times 10^{-11}$ | Yung et al. 1984 |
| R25b | | $\rightarrow C_2H_2 + C_2H_2$ | $3.3 \times 10^{-11}$ | Yung et al. 1984 |
| R26 | $C_4H + H + M$ | $\rightarrow C_4H_2 + M$ | $1.0 \times 10^{-30} \exp(457/T)$<br>$k_\infty = 5.0 \times 10^{-11}$ | Yung et al. 1984 |
| R27 | $C_4H + H_2$ | $\rightarrow C_4H_2 + H$ | $1.9 \times 10^{-11} \exp(-1762/T)$ | Yung et al. 1984 |
| R28 | $C_4H + CH_4$ | $\rightarrow C_4H_2 + CH_3$ | $2.2 \times 10^{-12} \exp(-503/T)$ | Yung et al. 1984 |
| R29 | $C_4H + C_2H_6$ | $\rightarrow C_4H_2 + C_2H_5$ | $6.0 \times 10^{-12} \exp(-302/T)$ | Yung et al. 1984 |
| R30 | $C_4H + C_2H_2$ | $\rightarrow C_6H_2 + H$ | $1.67 \times 10^{-11}$ | Yung et al. 1984 |
| R31 | $C_2H + C_4H_2$ | $\rightarrow C_6H_2 + H$ | $3.1 \times 10^{-11}$ | Yung et al. 1984 |
| R32 | $C_2H + C_4H_2$ | $\rightarrow C_6H_2 + H$ | $1.0 \times 10^{-11}$ | Yung et al. 1984 |
| R33 | $C_4H_2^{**} + C_4H_2$ | $\rightarrow C_8H_2 + H_2$ | $9.0 \times 10^{-11}$ | estimated to be collisional rate |

powered by the large solar flux in the Lyman-α line. This produces approximately equal quantities of $^1CH_2$ and $^3CH_2$. These radicals then react rapidly with $H_2$ and H to produce principally $CH_3$. Direct production of $CH_3$ from methane photolysis is forbidden by quantum mechanical theory, and has been confirmed by laboratory experiments (Slanger 1982). The other direct photolysis product of methane is the CH radical, which quickly reacts with methane to produce ethylene.

The primary fate of the methyl radical is to recycle to $CH_4$, but it also self reacts to produce $C_2H_6$. Ethane is chemically stable; it is destroyed only by photolysis, producing acetylene or ethylene, or it is removed by eddy mixing. Photolysis proceeds slowly from $C_2H_6$ because it absorbs solar ultraviolet in essentially the same spectral region as methane. Thus, $CH_4$ acts as an ultraviolet shield for ethane allowing its relative abundance to build up before its eventual removal by eddy mixing.

Ethylene is produced by the above reactions and from the $C_2H_3$ self reaction. It is destroyed rapidly by reacting with H, and by photolysis. Unlike ethane, ethylene has a significant absorption cross section beyond the methane cutoff at 1500 Å, so photolysis is not hampered by methane shielding.

Acetylene produced from both $C_2H_6$ and $C_2H_4$ photolysis is removed principally by photolysis and eddy mixing. Acetylene, like ethylene, has a significant absorption cross section in the ultraviolet beyond the methane cutoff. After photolysis, acetylene is either recycled or is converted to $C_4H_2$. Due to the low temperatures and low methane abundance on Uranus, a significant portion of the $C_2H_2$ is converted to diacetylene.

After undergoing photolysis, diacetylene either reproduces acetylene, recycles, or reacts to produce higher-order polyynes. The reaction scheme is similar to the one of Yung et al. (1984), but makes use of the recent laboratory measurements of Glicker and Okabe (1987) for the absorption cross section and quantum yields of $C_4H_2$ photolysis. Unfortunately, there are no laboratory measurements of the reactions involving the $C_4H$ radical or of $C_2H$ with $C_4H_2$. These reaction rates have been estimated in the manner of Yung et al. The reaction of ground-state $C_4H_2$ with its metastable excited state has been assumed to be the collisional rate. The lifetime of the metastable excited state of $C_4H_2$ against radiative relaxation has been assumed to be 1 millisec. The data of Glicker and Okabe yield only a lower limit, and the 1 millisec lifetime represents an upper limit.

Besides the above-mentioned photochemistry, there is a condensation sink for $C_4H_2$, $C_2H_2$ and $C_2H_6$. The vapor-phase loss rate of a condensing species is equal and opposite in sign of the diffusive growth rate for ice crystals; vapor phase molecules strike an ice crystal and stick to it. The diffusive mass growth rate (g $s^{-1}$ per crystal) is (Pruppacher and Klett 1980)

$$\frac{dm}{dt} = \frac{4\pi CSV_p D' M}{RT} \qquad (1$$

where $C$ is a parameter proportional to the crystal size and a function of the crystal geometry, $S$ is the degree of supersaturation, $T$ is the absolute temperature, $R$ is the universal gas constant, $V_p$ and $M$ are, respectively, the vapor pressure and the molecular weight of the condensing species, and $D'$ is the molecular diffusion coefficient of the condensing species corrected for gas kinetic effects for small crystals;

$$D' = \frac{D}{\frac{C}{C+\delta} + \frac{D}{C\alpha}\left(\frac{2\pi M}{RT}\right)^{1/2}}. \quad (2)$$

Here $\delta$ is the "thermal jump distance" which is on the order of the mean free path of the atmospheric molecules, $\alpha$ the sticking efficiency and $D$ the standard molecular diffusion coefficient. For small crystals, the second term in the denominator of Eq. (2) dominates and the crystal grows proportional to $C^2$; for large crystals, the first term dominates and $D'$ approaches the limit of $D$ and the crystal grows as only $C$. The column ice haze production rate is controlled by the column photochemical production of that species and the condensation loss rate adjusts the supersaturation to match this. So, any uncertainty in $\alpha$ or $C$ due to crystal geometry introduces an uncertainty in the supersaturation.

Equation (1) is a loss rate per crystal; to convert it into a loss rate needed in a photochemical model (molecules $cm^{-3}$ $s^{-1}$), a crystal surface area per unit volume or a number density profile of ice crystals is required. There are two ways to do this. From observations of the optical depth of the stratospheric haze layer (Pollack et al. 1987), a crystal surface area per unit volume can be inferred (Summers and Strobel 1989), or it can be assumed that all the downward transport of the condensing hydrocarbon through the cold trap is by ice crystal sedimentation (Romani and Atreya 1989). At equilibrium the photochemical column production rate of each species is balanced by the column density of aerosols times an inverse-lifetime. The lifetime is on the order of the time for the aerosols to fall from their condensation levels to the tropopause. The fall time is a function of the crystal size, so for each assumed ice-crystal size there is a corresponding column density. The column distribution is converted into a height distribution by assuming a particular distribution for the aerosols, e.g., uniform with height, exponential, etc.

The sink for the $C_6H_2$ and $C_8H_2$ produced in the above photochemistry is also likely to be condensation to their respective ices. Presently, there are no published measurements of the vapor pressures of these substances. However, the vapor pressure of $C_4H_2$ is lower than that of $C_2H_2$ by over 11 orders of magnitude at 75 K. Assuming a similar drop from $C_4H_2$ to $C_6H_2$ and $C_8H_2$, it seems likely that their fate is condensation.

The distribution of methane and its photolysis products are obtained by solving one-dimensional coupled continuity equations. The models assume a

steady-state condition and a horizontally averaged atmosphere, so the continuity equation for the $i^{th}$ species becomes

$$\frac{dF_i}{dz} = P_i - L_i \tag{3}$$

where $z$ is the altitude, $F_i$ is the flux of species $i$ in molecules $cm^{-2}\ s^{-1}$, $P_i$ is the chemical production rate and $L_i$ is the chemical loss rate of species $i$, both in units of molecules $cm^{-3}\ s^{-1}$. Species that potentially have long chemical lifetimes such as $CH_4$, $C_2H_2$, $C_2H_4$, $C_2H_6$ and H are allowed to undergo transport and chemical reactions, while short-lived species, such as the chemical radicals, are assumed to be in photochemical equilibrium.

The flux term in the continuity equation used in one-dimensional numerical models includes contributions from both eddy mixing and molecular diffusion. This is because the region of interest for methane photochemistry extends from the tropopause, where the atmosphere is well mixed, to the methane homopause. This expression for the flux of the $i^{th}$ species, $F_i$, is as follows:

$$F_i = n_i \left[ -D_i \left( \frac{1}{n_i}\frac{dn_i}{dz} + \frac{1}{H_i} + \frac{1}{T}\frac{dT}{dz} + \frac{\alpha_T}{T}\frac{dT}{dz} \right) - K \left( \frac{1}{n_i}\frac{dn_i}{dz} + \frac{1}{H_a} + \frac{1}{T}\frac{dT}{dz} \right) \right] \tag{4}$$

where subscripts $i$ and $a$ refer to the constituent $i$ and the bulk atmosphere, respectively; $D$ and $K$ are, respectively, the molecular and eddy diffusion coefficients; $\alpha_T$ is the thermal diffusion factor (which is a dimensionless quantity, unlike $D$ and $K$); $H$ is the scale height; $n$ is the number density; and $T$ is the atmospheric temperature. The molecular diffusion coefficients for the hydrocarbons and atomic hydrogen in $H_2$ and He are listed in Table IV. These background-gas-dependent diffusion coefficients are then combined to produce effective diffusion coefficients for each species in the model atmosphere. In the middle atmosphere $\alpha_T$ is generally negligible. Since the inference of $K$ on Uranus relies heavily on photochemistry, its discussion is deferred to the next section.

Boundary conditions and values for each species are also part of any numerical model. For Uranus, the natural boundary levels for methane photochemistry are the methane homopause and the tropopause. At the homopause, molecular diffusion becomes fast for the hydrocarbons and they follow their individual scale heights; so the upper boundary condition for the hydro-

**TABLE IV**
**Molecular Diffusion Coefficients[a]**
**Background Gas**

| Diffusing Species | $H_2$ | | He | | Reference |
|---|---|---|---|---|---|
| | *A* | *s* | *A* | *s* | |
| $CH_4$ | 2.30 | 0.765 | 2.30 | 0.750 | Marrero and Mason 1972 |
| $CH_3$ | 2.30 | 0.765 | 2.30 | 0.750 | assumed to be the same as $CH_4$ |
| $C_2H_2$ | 1.38 | 0.834 | 8.70 | 0.50 | for $H_2$, Weisman 1964; for He, Seuman and Ivakin 1961 |
| $C_2H_4$ | 1.62 | 0.791 | 4.01 | 0.618 | for $H_2$, Weisman 1964; for He, Frost 1967 |
| $C_2H_6$ | 2.01 | 0.738 | 3.35 | 0.633 | for $H_2$, Weisman 1964; for He, Frost 1967 |
| $C_4H_2$ | 1.44 | 0.750 | 1.24 | 0.750 | estimated using techniques given in Reid et al. 1977 |
| H | 8.30 | 0.728 | 1.04 | 0.732 | Marrero and Mason 1972 |

[a]The molecular diffusion coefficient for each species in the background gas in $cm^2s^{-1}$ is given by the formula; $D = 10^{17}AT^s/N$ where $T$ is the temperature in K and $N$ is the atmospheric number density in molecules $cm^{-3}$. The effective diffusion coefficient in the atmosphere $D_{eff}$ is: $D_{eff} = 1/(f_{H_2}/D_{H_2} + f_{He}/D_{He}$ where $f_{H_2}$) is the mixing ratio of $H_2$, $D_{H_2}$ is the molecular diffusion coefficient for the species in $H_2$, and $f_{He}$ and $D_{He}$ are the same for He.

carbons is zero net flux for each species. However, there is a source of atomic hydrogen above this level from electron impact on $H_2$ which results in a net downward flux of H through this boundary of approximately $3 \times 10^7$ hydrogen atoms $cm^{-2}\ s^{-1}$. At the tropopause, $CH_4$ is close to or below its saturation value (Lindal et al. 1987; Orton et al. 1987*b*). The acetylene and ethane mixing ratios are very close to their saturation values, while $C_4H_2$ is supersaturated due to its low vapor pressure (see discussion in Sec. III.B.2). $CH_3$, $C_2H_4$ and H are in local photochemical equilibrium at the lower boundary, and their boundary values are set accordingly.

Care must be taken in comparing the results of one-dimensional models to observations. One-dimensional models produce mixing-ratio profiles that are global averages while the Voyager UVS observations refer to specific latitudes. Earth-based observations in the infrared and ultraviolet of $CH_4$, $C_2H_2$ and $C_2H_6$ (Orton et al. 1987*b*; Caldwell et al. 1988) are global averages but report mixing ratios for an assumed height distribution. As will be seen in the next section, the height profile produced by the photochemical models are different from those assumed in the papers by Orton et al. and Caldwell et al.

### B. Results and Discussion

The following mixing ratio profiles were generated with the model of Romani and Atreya (1989). As noted above, Summers and Strobel (1989)

have published a similar model. Because of the sensitivity of condensation level to temperature, the assumed thermal structure is presented in Fig. 8. Below 0.3 mbar, the thermal profile is a smoothed version of the Voyager Radio Science Subsystem (RSS) occultation profile (Lindal et al. 1987); above it merges with the best-fit profile from the Voyager UVS (Herbert et al. 1987, their "b" profile).

*1. Hydrocarbon Mixing Ratio Profiles.* The mixing ratio profiles of methane and acetylene as a function of the eddy diffusion coefficient at the latitude of the solar occultation observed by the Voyager 2 UVS are shown in Figs. 9 and 10. For these studies $K$ was assumed to be inversely proportional to the square root of the atmospheric number density (see Sec. IV). These model-generated hydrocarbon profiles were then used by Herbert et al. (1987) to construct lightcurves to compare with the Voyager 2 UVS observations. As can be seen in these figures, the mixing ratio profiles are a strong function of $K$, with higher rates of eddy mixing transporting methane to higher levels in the atmosphere before photolysis can destroy it.

At pressures $> 0.05$ mbar, eddy mixing is faster than photolysis for $CH_4$ (assuming $K = 10^4$ cm$^2$s$^{-1}$ at the homopause after Herbert et al. [1987]), so its mixing ratio profile is controlled by eddy mixing. At this level, optical depth of one (slant path) is reached in Lyman-$\alpha$ and photolysis depletes the methane mixing ratio relative to its tropopause value. This occurs below the

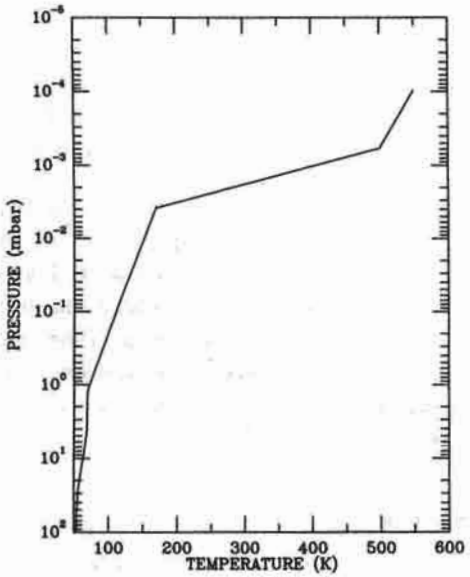


Fig. 8. Adopted thermal structure for the stratosphere of Uranus, based upon smoothed RSS thermal profile and Herbert et al. (1987; "b" in their Fig. 7) thermal profile.

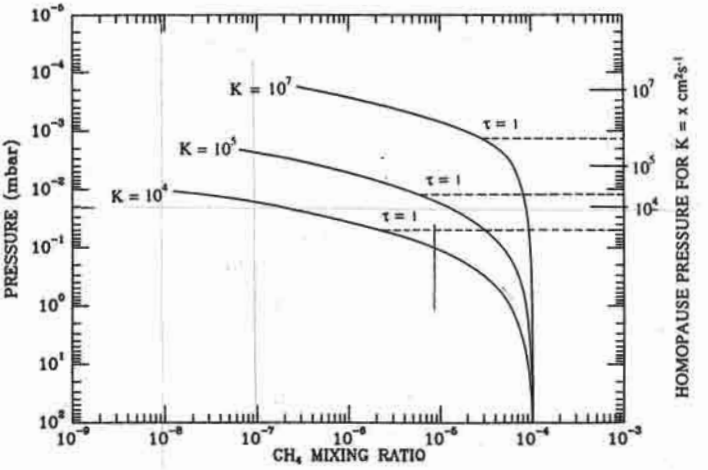


Fig. 9. The mixing-ratio profile of methane as a function of the eddy mixing coefficient at the latitude of the solar occultation observed by the Voyager 2 UVS. The value given for $K$ is the value it has at the methane homopause. $K$ is assumed to be proportional to the inverse square root of the atmospheric number density. The homopause levels for different $K$'s are marked on the right ordinate. The corresponding $\tau = 1$ levels for $CH_4$ at Lyman $\alpha$ are indicated on the curves.

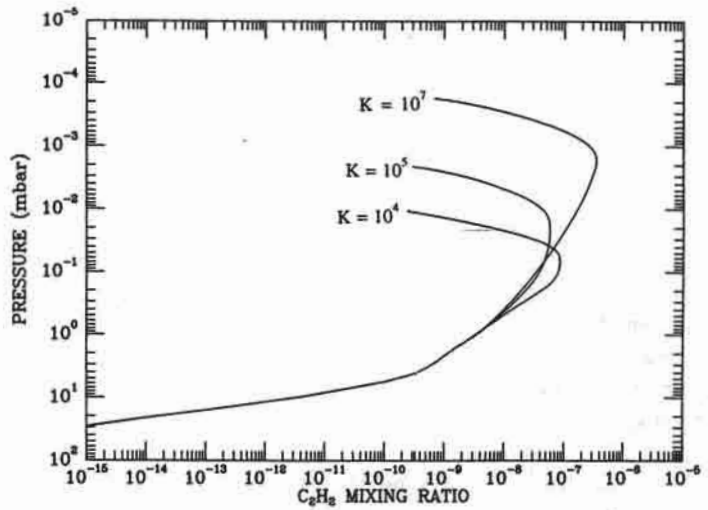


Fig. 10. Same as Fig. 9, except for acetylene

homopause because photodissociation becomes faster than eddy mixing at this level for these low values of the eddy diffusion coefficient. The eddy mixing time is on the order of $4 \times 10^9$ s, while the photolysis loss lifetime is on the order of $5 \times 10^8$ s. Above the homopause (0.02 mbar), molecular diffusion takes over from chemistry in controlling the methane profile.

Methane photolysis is relatively inefficient on Uranus. Only 10 to 15% of $CH_4$ molecules which absorb ultraviolet photons go on to produce $C_2$ or higher-order hydrocarbons, resulting in a loss rate of $6 \times 10^6$ methane molecules $cm^{-2}\ s^{-1}$ at the equator. For comparison, the loss rate on Jupiter is 30% (Gladstone 1982). The lower loss rate on Uranus is also a result of the lower eddy mixing rate. Reactions that lead to the recycling of methane are favored by high number densities.

Chemical production and loss (including condensation) are faster than eddy mixing at all levels for acetylene below the homopause. However, the chemical lifetimes are never fast enough to dominate completely over transport. Primary production of $C_2H_2$ from $C_2H_4$ and $C_2H_6$ photolysis peaks at the 0.05 mbar level but the peak in the $C_2H_2$ mixing ratio occurs slightly below due to transport and a secondary peak in production from recycling from $C_4H_2$ at 0.15 mbar. Below this level the acetylene mixing ratio diminishes with increasing pressure, owing to loss by photolysis and transport down to the condensation sink. About 40% of the time that $C_2H_2$ undergoes photolysis, it goes on to produce $C_4H_2$. Below 1.5 mbar ($\approx$69 K), $C_2H_2$ condenses to its ice, and its mixing ratio follows the saturation profile. If there were insufficient numbers of ice crystals for $C_2H_2$ to condense on, acetylene would become highly supersaturated so the condensation loss would balance the flux of acetylene into the condensation region from above and *in situ* chemical production. In the work discussed in Romani and Atreya (1989) and here, the ice crystals are uniformly distributed with height and $C_2H_2$ is allowed to condense on only its own ice crystals (i.e., homogeneous nucleation), and the supersaturations are in the range of 5 to 10%. Summers and Strobel (1989) also found that acetylene never became highly supersaturated in its condensation region.

In the previous figures, the methane mixing ratio at the lower boundary (tropopause: 53 K, 100 mbar) was at its saturation value, $10^{-4}$. Lindal et al. (1987) found that their data from the radio occultation at the equator are consistent with $CH_4$ at 30% of saturation in the stratosphere. Orton et al. (1987), from infrared observations at 8 μm, place an upper limit on $CH_4$ at $10^{-5}$ in the stratosphere, i.e., 10% of saturation or less. These lower-than-saturation values of the methane mixing ratio may be due in part to where $CH_4$ is transported into the stratosphere. From analysis of Voyager IRIS data, Flasar et al. (1987) found only two minima in tropopause temperatures with latitude, and thus only two regions where transport through the troposphere could occur (25° S and 40° N). The stronger minimum at 25° S (49 K) would produce a methane saturation mixing ratio of $1.8 \times 10^{-5}$. In Fig. 11 the mixing ratio profiles of methane and acetylene are shown for $CH_4$ at saturation (solid lines) and at 30% of saturation (dashed lines). The possibility of subsaturated methane is not yet fully established. If it is indeed viable, then its effect on inferences of aeronomic properties, such as mixing, must be taken into account.

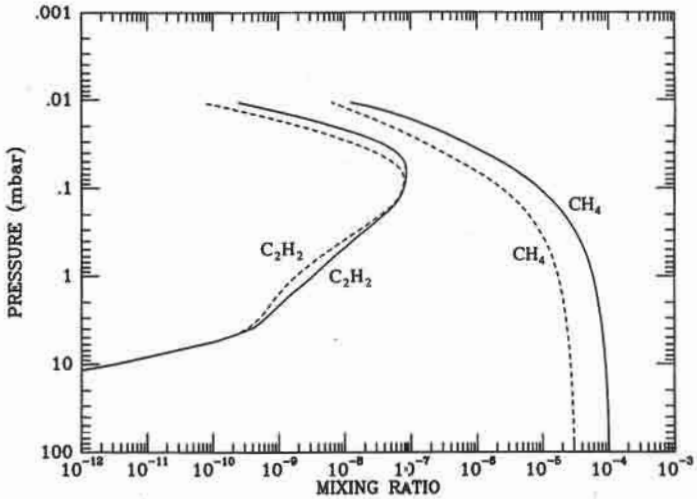


Fig. 11. The mixing-ratio profiles of $CH_4$ and $C_2H_2$ for two different $CH_4$ mixing ratios at the tropopause (cold trap). The solid line is for saturated $CH_4$; the dashed line is for $CH_4$ at 30% of saturation.

In Fig. 12, the methane and acetylene profiles at the subsolar point are shown with the same eddy mixing coefficient as deduced by Herbert et al. (1987) from the solar occultation at the equator (solid lines). Yelle et al. (1987*a*), in an analysis of the Raman-scattered solar Lyman-α line in UVS spectra at the south pole of Uranus, require that the hydrocarbons be absent above the 0.5 mbar level (column abundance of hydrocarbons $< 5 \times 10^{16}$ molecules $cm^{-2}$). While the reduction in the slant path from the equator to the pole lowers the level where methane is photolyzed, it is insufficient to remove the hydrocarbons from above the 0.5 mbar level. For comparison, also in Fig. 12, the mixing ratio profiles of $CH_4$ and $C_2H_2$ which match the Raman-scattered solar Lyman-α line are shown (dashed lines). This model was calculated with a constant eddy diffusion coefficient of 200 $cm^2\ s^{-1}$, as deduced by Yelle et al. (1987*a*). Subsequently, Yelle et al. (1989) analyzed the far-ultraviolet solar reflection spectrum of Uranus obtained from Voyager UVS data. These data also came from observations at the south pole. They require even lower hydrocarbon mixing ratios than Yelle et al. (1987*a*); above 3 mbar, a $CH_4$ mixing ratio of (1–3) $\times\ 10^{-7}$ and a $C_2H_2$ mixing ratio of (0.6–1.2) $\times\ 10^{-8}$, and between 3 and 5 mbar, respectively, mixing ratios of $3 \times 10^{-7}$ and (0.6–2) $\times\ 10^{-8}$. This requires an eddy diffusion coefficient of 50 $cm^2\ s^{-1}$ (constant) or 1500 $cm^2\ s^{-1}$ (varying inversely with the square root of the atmospheric number density) at the methane homopause (Summers and Strobel 1989). Thus the observed latitude variation in hydrocarbons cannot be explained by a one-dimensional photochemical model with latitude independent *K* and chemistry.

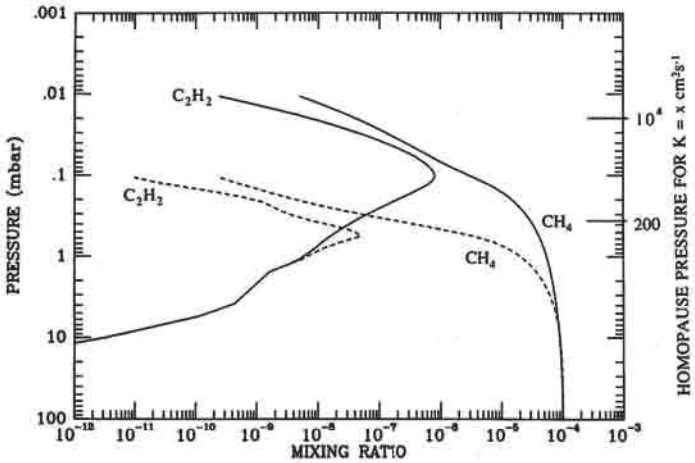


Fig. 12. The mixing-ratio profiles of $CH_4$ and $C_2H_2$ at the sunlit pole of Uranus. The solid lines are for a $K_z$ of $10^4$ $cm^2$ $s^{-1}$ and are proportional tc the inverse square root of the atmospheric number density—deduced from the UVS solar occultation experiments at 4° S (Herbert et al. 1987); the dashed lines are for a constant $K$ of 200 $cm^2$ $s^{-1}$ as deduced by Yelle et al. (1987*a*) from analysis of Raman scattered Lyman-α emissions at the south pole of Uranus. The homopause levels for the two cases are indicated on the right ordinate.

Yelle et al. (1989) suggested that this latitude variation is due to horizontal transport. Adopting the circulation pattern deduced from the Voyager 2 IRIS observations (Flasar et al. 1987), methane is injected into the stratosphere in the sunlit hemisphere only at 25° S and is destroyed photochemically on its journey poleward. Equatorward, the destruction rate is slower due to the reduced solar flux. Model calculations by Flasar et al. (1987) gave a vertical velocity of $5 \times 10^{-4}$ cm $s^{-1}$ in the lower stratosphere. This can be scaled to give a horizontal velocity of ~0.1 cm $s^{-1}$ or a pole-to-equator transport time of $2.4 \times 10^{10}$ s. This is about nine Uranian years and longer than the lifetime of a methane molecule against photolysis at the $\tau = 0$ level. The $CH_4$ column destruction rate in the sunlit hemisphere of Uranus is on the order of $5 \times 10^7$ molecules $cm^{-2}$ $s^{-1}$. At this rate, and assuming an initial $CH_4$ height distribution given by a model with equatorial $K = 10^4$ $cm^2$ $s^{-1}$ (Herbert et al. 1987), all of the hydrocarbons above 0.3 mbar would be removed. Using a somewhat longer transport time of $10^{11}$ s, Yelle et al. (1989) find that all of the hydrocarbons above 0.5 mbar would be removed.

In addition to the ultraviolet induced destruction of methane during transport poleward, there will also be loss caused by charged-particle bombardment in the auroral zones. Thompson et al. (1987*a*) estimated the production rate of hydrocarbons in the auroral zone on Uranus from $CH_4$-$H_2$-He irradiation experiments. To balance their hydrocarbon production rate, the methane destruction rate has to be on the order of $2 \times 10^8$ molecules $cm^{-2}$ $s^{-1}$ in the auroral zone. Adding this loss rate to the one from the solar ultra-

violet would remove the hydrocarbons above the 0.8-mbar level for a transport time of $2.4 \times 10^{10}$ s, or 1.5-mbar level for a transport time of $10^{11}$ s. This is an upper limit of the methane destruction rate as the auroral zone is approximately 0.06 to 0.1 of the dayside hemisphere on Uranus. Since these simple latitude transport and photochemical destruction arguments do not entirely account for the observed variation in the hydrocarbons, more detailed two-dimensional modeling is required. It may also be that the sunlit pole on Uranus is somehow dynamically isolated from the rest of the stratosphere so that, rather than a smooth decrease of the hydrocarbons from the injection latitude to the pole, there is a discontinuity.

It must be pointed out that Flasar et al. (1987) used a simple dynamical model which assumes that radiative damping is independent of latitude, which may not be the case. The circulation pattern is based upon the thermal structure retrieved from IRIS observations that are sensitive only to the 10- to 1000-mbar pressure region, while the ultraviolet observations are sensitive to hydrocarbons above this level. The vertical scale for the meridional mass flux is only one scale height; it is not certain that this circulation persists above the 10-mbar level (M. Flasar, personal communication, 1988). On Jupiter, the only outer planet where there is good height information on the lower stratospheric thermal structure, the horizontal contrast in the temperature reverses itself above 10 mbar for reasons not yet known (Flasar et al. 1981; Conrath et al. 1981). There will also be feedback between the hydrocarbon vertical distribution and the dynamics as $CH_4$ is the major heater in the stratosphere and $C_2H_2$ the major cooler (B. J. Conrath, personal communication, 1988). At this time the observed latitude variation of the height profiles of the hydrocarbons is not understood. Better modeling of auroral chemistry and two-dimensional photochemical modeling are needed to address this problem.

Influx of micrometeorites or material from the Uranian rings and the moons might alter the $CH_4$ chemical cycle and, consequently, the composition of trace constituents in the stratosphere. The latter play an important role in determining the atmospheric thermal structure. Water and methane (or their derivatives) are the likely infalling material. If a material is charged, as is likely for ring or moon material passing through the magnetosphere, it enters the Uranian upper atmosphere along magnetic field lines. One thus expects to find relatively large quantities of such material near the magnetic pole (the magnetic pole is offset from the equator by approximately 15°). Redistribution of the material to other latitudes will be accomplished by the upper atmospheric wind system. Oxygen-bearing material (such as $H_2O$) would enter the $CH_4$ chemical cycle and lead to the formation of two important trace constituents: formaldehyde (HCHO) and carbon monoxide (CO). Carbon monoxide has been detected on Jupiter and Saturn. However, these observations favor an intrinsic source of CO over an extraplanetary source (Noll et al. 1986). Any incoming hydrocarbons ($CH_4$ or its derivatives from the ring/

moon surfaces) will have little impact on the $CH_4$ chemistry of Uranus. However, they might be important condensation nuclei for the condensing species in the stratosphere and troposphere of Uranus.

*2. Hydrocarbon Ice Hazes.* Figure 13 shows a comparison between the mixing-ratio profiles of the $C_2H_2$, $C_2H_6$ and $C_4H_2$ generated from the photochemical-condensation model (solid lines) and those allowed by saturation equilibrium above their respective ices (dashed lines). The haze formation levels are given in Table V. It is important to note that the actual formation levels depend strongly upon the local temperature. The vapor pressures depend exponentially upon temperature, so changes on the order of 5 K result in order-of-magnitude changes in the allowed abundances. Unfortunately, in the haze formation region, 15 mbar to 0.05 mbar, the thermal structure of Uranus is not known within ± 5 K, nor is there much information on the latitudinal structure of the thermal profile. Analysis of Voyager photopolarimeter measurements at 69° N (night side of Uranus) by West et al. (1987) yielded temperatures of 85 ± 2.3 K at 2.7 mbar and 90 ± 6 K at 1 mbar. These are much warmer than the temperatures used in the models discussed in this chapter, 69 K at 2.7 mbar and 74 K at 1 mbar. The steep gradients in the saturation mixing ratios seen in Fig. 13 at 1 to 3 mbar are the effects of the adopted thermal profile (Fig. 8). Care must be taken when comparing the predicted haze formation levels to other model atmospheres; it is the temperature levels that should be compared, not the pressure levels.

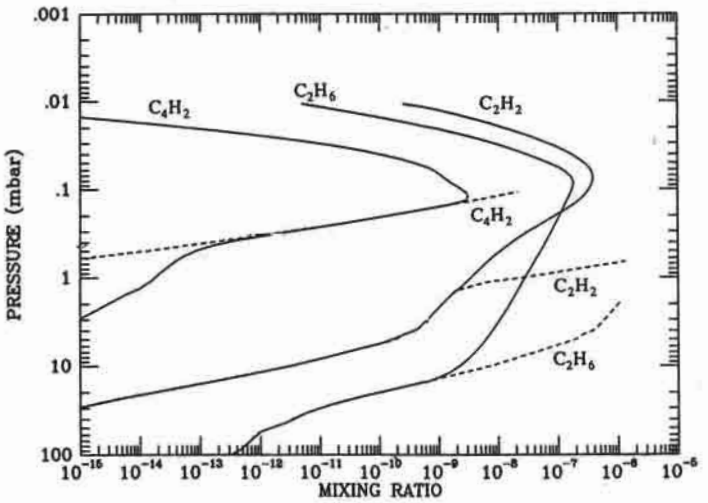


Fig. 13. The mixing-ratio profiles of $C_2H_6$, $C_2H_2$ and $C_4H_2$ from the photochemical-condensation model (solid lines) compared to their respective saturation mixing-ratio curves (dashed lines). The model is run with equatorial $K_h = 10^4$ cm$^2$ s$^{-1}$ and for a latitude of 15° S, to compare to the high phase-angle observations of the Voyager 2 imaging system.

**TABLE V**
**Condensation Levels at Uranus[a]**

| Species | Temperature (K) | Pressure (mbar) |
|---|---|---|
| $C_6H_2$ | <105 | <0.15 |
| $C_4H_2$ | 105 | 0.15 |
| $C_2H_2$ | 69 | 1.5 |
| $C_2H_6$ | 60 | 15.0 |

[a]These are the levels at which the hydrocarbons first begin to condense to their ices, with the exception that it is assumed that $C_6H_2$ condenses everywhere as soon as it is formed.

Of all the condensing species, only $C_4H_2$ shows substantial supersaturation. The $C_4H_2$ ice haze is primarily produced *in situ* with photochemical production balanced by condensation loss at each level in the model. The photochemical production of $C_4H_2$ drops by only 2 orders of magnitude from the top of its haze production layer to ~ 4-mbar level. However, its allowed saturation mixing ratio drops by 10 orders of magnitude in the same pressure range. As can be seen in Eq. (1), this balancing of photochemical production by condensation loss requires the supersaturation to grow by 8 orders of magnitude. Below 4 mbar, the $C_2H_2$ mixing ratio drops precipitously due to condensation and thus the $C_4H_2$ production rate drops. The $C_4H_2$ supersaturation accordingly drops, and the model mixing ratio returns to the supersaturation curve.

On Uranus, it is the formation and subsequent sedimentation of these hazes that balances the photolytic destruction of methane in the stratosphere. Ethylene and the radicals are in photochemical equilibrium and do not contribute to the downward flux. Ice haze production for a given species consists of both flux into, and photochemical production within, the condensation region. The haze production rates for 15° S are summarized in Table VI (this latitude was chosen to compare model predictions to high-resolution Voyager 2 images). These production rates are higher than values given previously using an earlier version of this model (Pollack et al. 1987). Previously, all of

**TABLE VI**
**Haze Production Rates at Uranus (g cm$^{-2}$ s$^{-1}$)[a]**

| Species | Flux into Condensation Region | *In Situ* Production | Total |
|---|---|---|---|
| $C_6H_2$ | 0.0 | $8.8 \times 10^{-17}$ | $8.8 \times 10^{-17}$ |
| $C_4H_2$ | $2.9 \times 10^{-17}$ | $3.4 \times 10^{-16}$ | $3.7 \times 10^{-16}$ |
| $C_2H_2$ | $1.1 \times 10^{-17}$ | $3.0 \times 10^{-17}$ | $4.1 \times 10^{-17}$ |
| $C_2H_6$ | $5.0 \times 10^{-17}$ | $2.3 \times 10^{-17}$ | $7.3 \times 10^{-17}$ |

[a]Calculated from photochemical model for 15° S latitude; total mass production rate = $5.7 \times 10^{-16}$ g cm$^{-2}$s$^{-1}$.

the haze producing species were not taken properly into account, notably $C_4H_2$ and $C_6H_2$.

The Voyager 2 imaging system provided clear evidence of aerosols in the stratosphere of Uranus (chapter by West et al.; Pollack et al. 1987). As mentioned above, methane and its photochemical products are the only likely sources of hazes in the stratosphere of Uranus because other possible haze candidates ($NH_3$ and $PH_3$) are removed by condensation well below the tropopause (West et al. 1986). Methane photochemical models predicted the locations of hazes and the haze-production rates in the atmosphere. Current analysis of high-resolution, low-latitude Voyager 2 images (combined radiative transfer and cloud microphysics modeling) indicates a haze formation rate of $1.0 \times 10^{-16}$ g cm$^{-2}$ s$^{-1}$ in the lower stratosphere (J. B. Pollack, personal communication, 1988), in reasonable agreement with the model-predicted values $5.7 \times 10^{-16}$ g cm$^{-2}$ s$^{-1}$. (Summers and Strobel [1989] report a mass production rate of $2 \times 10^{-16}$ g cm$^{-2}$s$^{-1}$. The difference between their model and the one discussed here is in the choice of eddy diffusion coefficient and a somewhat different chemical scheme.) Also, the haze forms at approximately the pressure region predicted by the models. The somewhat lower rate of haze formation, according to the observations, may be a consequence of horizontal transport of haze material as the haze production rate drops off rapidly towards the equator (see discussion below). Thus the location and production rates from the model agree with the observations, within model uncertainties.

However, the Voyager 2 observations require the haze material to be absorbing in the visible (Pollack et al. 1987). The haze materials are all initially white/colorless in the visible; $C_4H_2$ absorbs out to 2600 Å; and $C_6H_2$ absorbs out to 3000 Å, the longest wavelengths of absorption for the condensing species. A likely candidate for dark haze material is ultraviolet-induced polymerization in the acetylene and polyacetylene ices. Stief et al. (1965) observed hydrogen production from ultraviolet irradiation of $C_2H_2$ ice. In addition, a waxy substance was left behind after the irradiated $C_2H_2$ was allowed to evaporate (L.J. Stief, personal communication, 1987). Due to the low abundances of the hydrocarbons in the stratosphere of Uranus, the region of ice formation is exposed to radiation longward of 1430 Å, making this possible. Note, however, that this dark material cannot be a polyyne, as the polyynes out to pentaacetylene ($C_{10}H_2$) have been reported to be colorless crystalline solids (Kloster-Jensen et al. 1974). Also, Khare et al. (1987) have proposed that the source of the dark material is charged-particle bombardment of gas phase methane in auroral regions, producing solid hydrocarbons (tholins). However, their estimated global rate of production of solids, $4 \times 10^5$ carbon atoms cm$^{-2}$ s$^{-1}$ (approximately 2% of the photochemical conversion rate of $CH_4$ to hydrocarbon ices), coupled with the measured imaginary index of refraction of the material, makes this source too small to produce sufficient absorbing material. Thompson et al. (1987*a*) estimated the

global production rate of gas-phase hydrocarbons from charged-particle bombardment in the stratosphere of Uranus to be on the order of $10^6$ molecules $cm^{-2}\ s^{-1}$. About half of this is due to $C_2H_6$, and the remaining to $C_3H_8$ and $C_4H_{10}$. Ultraviolet irradiation of these last two hydrocarbons is also a potential source of dark material which needs to be quantified. Recently Colwell and Esposito (1989) have estimated an upper limit to the mass loss rate from the epsilon ring to the atmosphere of Uranus of $10^{11}$ g $year^{-1}$. This corresponds to a haze production rate of $4.0 \times 10^{-17}$ g $cm^{-2}\ s^{-1}$, about 1/10 of the photochemical rate. The ring material, unlike the photochemically produced material, is dark. However, its color is grey, while the dark component of the haze material is red. The infalling ring material then may not be a source of the dark component of the hazes, but is a likely source of condensation nuclei for the hydrocarbon ices produced by the methane photochemistry.

As the source of the hydrocarbon ices is the photochemical destruction of $CH_4$, the total haze production rate tracks with the incident solar flux density. For present conditions on Uranus, this means that the production rate increases by a factor of 16 from the equator ($1.4 \times 10^{-16}$ g $cm^{-2}\ s^{-1}$) to the pole ($2.2 \times 10^{-15}$ g $cm^{-2}\ s^{-1}$). A factor of 2 represents the change from a diurnal average of the solar flux at the equator to constant illumination at the pole, and the additional factor of 8 represents the variation of the cosine of the solar zenith angle. The composition of the haze also changes. Most of the increase is in $C_4H_2$ and $C_6H_2$ production, the two species that are produced predominantly *in situ*. At the equator, the haze production rate of these two species is 60% by mass, but at the pole it is 85%. Going from solar minimum to maximum results in an increase of a factor of 2 in production rate. This is due to the increase in the flux of the solar Lyman α line, the primary source of the photochemical destruction of methane. Once again, the composition changes with the $C_6H_2$ production increasing at most by a factor of 4 to 5.

During the 42 yr winter night on Uranus, production in the vapor phase of the condensing hydrocarbons ceases. Haze production continues, however, as $C_2H_2$ and $C_2H_6$ in the upper stratosphere are transported into the lower stratosphere where they condense out. The eddy mixing lifetime at 1 mbar is on the order of 3 Uranus years. Thus, haze production continues throughout the winter night, but at a much reduced rate ($\approx 5 \times 10^{-17}$ g $cm^{-2}\ s^{-1}$). Any production from charged-particle bombardment will of course continue.

The haze production rate is photon, not methane, limited. This is because the optical depth at the tropopause is in excess of $5 \times 10^3$, even for the low values of the methane mixing ratio corresponding to saturation equilibrium at the observed range of tropopause temperatures on Uranus. This photon-limited haze production also means that the formation rate is relatively insensitive to the eddy mixing coefficient. For the range of acceptable eddy mixing coefficients, the overall haze production rate remains approximately the same.

The above changes in haze production with solar activity, latitude, and

season can induce changes in the haze itself with the above parameters. These alterations in the haze will be reduced by the long residence time for the haze particles. For 0.1 μm-sized particles (approximately the observed modal radius; Pollack et al. 1987), the fall time is on the order of one Uranus year, much longer than the solar cycle.

## IV. VERTICAL MIXING

### A. Diffusion Equations

Mixing plays a central role in determining the distribution of constituents in a planetary atmosphere. Vertical mixing tends to homogenize the atmosphere, so that, in the absence of chemistry and condensation, all species attain the same common (atmospheric) scale height. The strength of vertical mixing is characterized by a parameter called the eddy diffusion coefficient $K$, which incorporates small-scale vertical motions (leading to turbulence) as well as vertical motions on a larger scale. The level in the atmosphere where the eddy diffusion coefficient equals the molecular diffusion coefficient is variously referred to as the turbopause or the homopause, the latter nomenclature being more representative of the phenomena in the context of planetary atmospheres. Molecular diffusion dominates above the homopause, constraining the constituents to be distributed according to their own "individual" scale heights, thus resulting in a more rapid drop in the density of the heavier constituents relative to the lighter ones. In addition to the eddy and molecular diffusion processes, termperature gradients produce thermal diffusion in the atmosphere.

The flux of a minor constituent diffusing through the atmosphere is given by Eq. (4), the flux equation (Sec. III). The distribution of the minor constituents in this equation is obtained by solving Eq. (3), the continuity equation (Sec. III). Whereas $D$ and $\alpha_T$ can be determined from gas kinetic considerations, the eddy diffusion coefficient must be derived indirectly from observational data on planetary atmospheres. Many techniques have been used to determine $K$ successfully for Jupiter, Saturn and Titan (Atreya et al. 1981; McConnell et al. 1981; Atreya 1982; Sandel et al. 1982; Smith et al. 1982; a review in Atreya 1986, pp. 66–79). These methods include the study of the dependence of hydrogen Lyman α (1216 Å) and He 584 Å intensities on the location of the homopause, hence $K$. In principle, the altitude where the $CH_4$ density drops rapidly should represent the homopause level. Once that level is known, the molecular diffusion coefficient of the given constituent can be calculated from the following formulation

$$D = \frac{3}{32\, Q_D\, n}\, \mathrm{v} \qquad (5)$$

where $Q_D$ is the mean momentum transfer cross section, $n$ is the background atmospheric number density, and v is the velocity of the constituent diffusing through the background gas.

The above-mentioned expression for $CH_4$ diffusing through $H_2$ reduces to

$$D = 10^{19} / n \text{ cm}^2 \text{ s}^{-1} \quad (6)$$

for a typical Uranian homopause temperature of 130 K (Atreya 1986, p. 78). For other diffusion coefficients see Atreya (1986), and Table IV here. In the middle atmospheres of the major planets, the thermal diffusion term is negligible. Since the eddy and molecular diffusion coefficients are equal at the homopause, by definition the value of the eddy diffusion at that level is fixed.

The above-mentioned method of determining the homopause level is valid, however, only if the distribution of the heavier gas under consideration is controlled *entirely* by transport. That would be the case for an inert gas such as argon, neon or helium. However, Voyager could not measure the height profiles of these gases. $CH_4$, on the other hand, undergoes photolysis, so its density begins to decline even at levels below the homopause, thus giving a false impression of the homopause level. Such behavior is readily apparent in Fig. 9, which shows that the homopause level for different values of $K$ is separated from the level of unit optical depth where most of $CH_4$ photodissociation occurs. Therefore, in order to determine $K$ from the $CH_4$ height profile, it is necessary to fold the measured $CH_4$ profile into the photochemical models, as the latter are dependent on $K$. A further complication arises at Uranus and Neptune. Because of the low temperatures prevalent in the middle atmospheres of these planets, most of the hydrocarbon products undergo condensation, primarily near the base of the stratosphere (see Sec. III). The photochemical models, therefore, need to account for the coupling between the gas and the condensed phases.

### B. Measurement of Eddy Diffusion Coefficient

By monitoring the height distribution of $CH_4$ it was possible to determine the value of eddy diffusion coefficient on Jupiter and Saturn. This technique is, however, not directly applicable to Uranus; this is primarily due to the fact that $CH_4$ distribution on Uranus could not be determined with any degree of accuracy. The reduced solar flux at Uranus, combined with the large projected size of the Sun (larger than the atmospheric scale height at Uranus) and the Lyman-$\alpha$ scattering into the $CH_4$-absorption channels, all contributed to this problem. The ultraviolet stellar occultations also were not useful for the middle atmosphere (>1-$\mu$bar region), primarily because of the low level of the photon flux (see Sec. II for a detailed discussion of the Voyager ultraviolet occultations).

The methane absorption channels in the Voyager ultraviolet solar occultations can still be used to obtain an approximate value of the eddy diffusion coefficient, as was done in Atreya et al. (1986) and Herbert et al. (1987). A more accurate determination of the value of $K$ in the atmosphere of Uranus is possible if one resorts to another hydrocarbon, such as acetylene, whose signature has been identified in the Voyager ultraviolet spectra (Sec. II). Acetylene absorbs to wavelengths much longer than $CH_4$ and $C_2H_6$ (an exception is $C_2H_4$—its abundance is, however, too low). The longer-wavelength lightcurves can thus be used to derive the eddy diffusion coefficient. Again, because of limited success in determining the height distributions, a direct comparison of the measurements with the modeled photochemical profiles was not possible. Instead, lightcurves themselves must be simulated. Figure 14 shows a comparison, at three different wavelength ranges, between the observed lightcurves and lightcurves synthesized from model photochemical profiles. The top panel in Fig. 14 shows absorption mainly by $CH_4$, with minor contributions from other hydrocarbons, $H_2$ Lyman and Werner bands, and $H_2$ Rayleigh scattering. Comparison between data and simulations in this

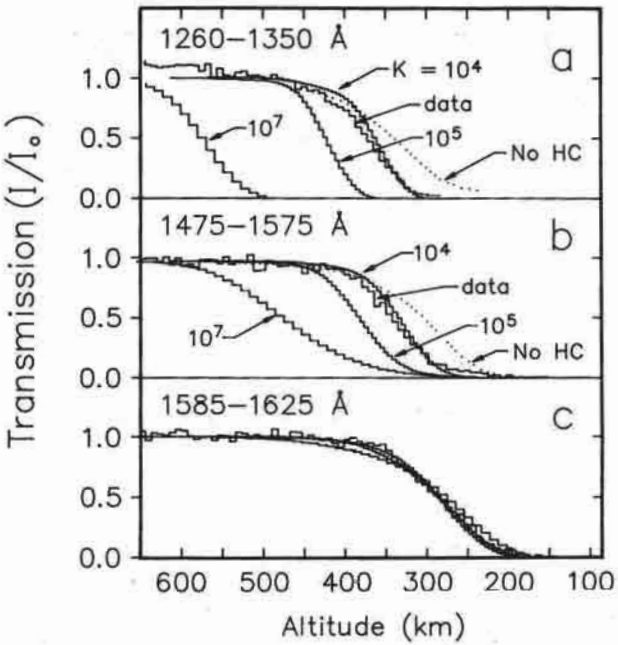


Fig. 14. Comparison of the model lightcurves with the observed ultraviolet occultation lightcurves. The models are based on a photochemical model in which the eddy diffusion coefficient is a free parameter. The best fit is for $K_h = 10^4$ cm$^2$s$^{-1}$. The dotted curves, (a) and (b) show the effect of pure Rayleigh scattering in $H_2$ without hydrocarbon absorption. In (c), simulations with different values of $K$ fall on top of one another and the data, as do the dotted curves (in Figs. 14a and 14b), as expected (Herbert et al. 1987).

panel indicates that the $K = 10^4$ cm$^2$ s$^{-1}$ case gives the best rough estimate of $K$ at the homopause. The bottom panel in Fig 14 represents essentially pure Rayleigh scattering by $H_2$, so that the choice of $K$ is immaterial; all simulations fall on top of one another, as expected. The middle panel in Fig 14 represents absorption by $C_2H_2$ and is the most diagnostic of $K$. The case with $K = 10^4$ cm$^2$ s$^{-1}$ again gives the best match between the data and the simulated lightcurves. Further refinement of the simulations is not warranted because of uncertainties in the data and the parameters of the model. The largest uncertainty is in the height variation of the eddy diffusion coefficient.

Although Jupiter and Saturn may not be completely parallel analogs to the vertical mixing in the atmosphere of Uranus, it is nevertheless instructive to note that in the atmospheres of the former two, the observed distributions of minor constituents (mainly hydrocarbons) are best explained with the assumption of $K$ varying approximately as the inverse square root of atmospheric number density, i.e.,

$$K \propto M^{-a} \tag{7}$$

where $a \approx 0.5$ (Atreya et al. 1981; McConnell et al. 1981; Atreya 1982; Sandel et al. 1982).

Behavior similar to that given by Eq. (7) is also valid for the upper atmosphere of the Earth (Hunten 1975; Lindzen 1971) but is by no means applicable in the lower atmosphere, particularly at the base of the stratosphere and in the troposphere. Many different combinations of $a$ and $K$ at the homopause $K_h$ were used in the simulations presented by Atreya et al. (1986) and Herbert et al. (1987), and the ones with $K_h \approx 10^4$ cm$^2$ s$^{-1}$ and $a \approx 0.5$ produced the best match to the data. Summers and Strobel (1989) find $K_h = 3 \times 10^3$ cm$^2$ s$^{-1}$ on the basis of their photochemical models and the Voyager data. Whether or not the apparent factor of 3 discrepancy between these results and those of Atreya et al. (1986) and Herbert et al. (1987) is real will require further analysis of the solar occultation data, and if possible, the stellar occultation data. Even then, it may not be possible to determine $K$ with more accuracy because the quality of the relevant Voyager data at Uranus is not as high as that at Jupiter and Saturn. Finally, Fig. 15 shows the variation of $K$ and $D$ in the atmosphere of Uranus. By definition, the two curves cross at the homopause, which is located at an atmospheric density level of $10^{15}$ cm$^{-3}$ where the atmospheric pressure is 20 μbar.

A comparison with Jupiter and Saturn (Table VII) shows that vertical mixing on Uranus is relatively sluggish. Such a low vertical mixing on Uranus is perhaps related to Uranus' relatively small internal energy source and much lower (than Jupiter and Saturn) combined energy input to the atmosphere from the Sun and the magnetosphere.

A highly stable tropopause at Uranus with weak turbulence and a Richardson number greater than 1000 was predicted by Stone (1975). This would

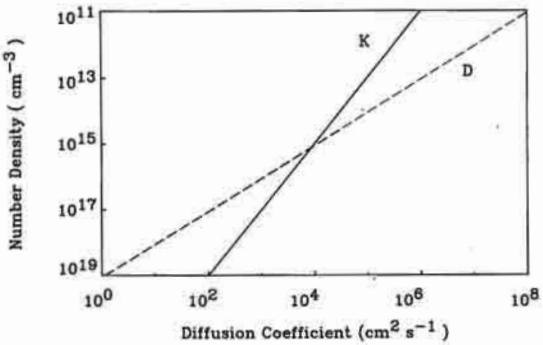


Fig. 15. Variations of eddy diffusion $K$ and the molecular diffusion $D$ coefficients with atmospheric number density $M$, assuming the measured value of $K = 10^4$ cm$^2$s$^{-1}$ at the homopause. As expected, the $K$ and $D$ curves cross for $K = D = 10^4$ cm$^2$s$^{-1}$, giving the location of the methane homopause at an atmospheric density level of approximately $10^{15}$ cm$^{-3}$ (20 μbar on Uranus).

result in small eddy mixing vertically. As mentioned in Sec I, the small-scale features in the temperature profile obtained from groundbased stellar occultation observations can be explained in terms of the vertically propagating gravity waves, and such propagation would require a relatively low value of $K < 3 \times 10^4$ cm$^2$ s$^{-1}$ in the 0.3 to 30 μbar region.

Finally, there is an indication of possible latitudinal variation in $K$. The detection of Raman scattered emission at 1280 Å in the subsolar region implies approximately a factor of 100 smaller $CH_4$ mixing ratio relative to the photochemical predictions in the 3 mbar region (Sec II). A simple explanation would be that the eddy diffusion coefficient is low, 100 to 350 cm$^2$ s$^{-1}$, not just in the 0.5 to 100 mbar region, as suggested by Yelle et al. (1987*a*), but throughout the atmosphere—in fact, $K$ of 100 to 350 cm$^2$ s$^{-1}$ in the 0.5 to 100 mbar is consistent with $K_h = 10^4$ and its variation according to Eq. (7). On the other hand, the "equatorial" thermal structure is consistent with nearly saturated concentrations of $CH_4$ (J. Appleby, personal communication, 1988), not the depleted values implied by the ultraviolet reflection spectroscopy data taken at the polar latitudes. Unless the results of two-dimensional photochemical modeling prove otherwise, it appears that the discrepancy between the results of solar occultation (equatorial) and the reflection spectra (polar) is indicative of a true latitudinal variation in the hydrocarbon distributions. This does not rule out entirely some latitudinal variation in the strength of atmospheric vertical mixing.

## V. CONCLUSIONS

Photolysis of methane in the atmosphere of Uranus produces heavier hydrocarbons, the most abundant of which are ethane, acetylene and the po-

**TABLE VII**
**Eddy Diffusion Coefficient**

| | Homopause Characteristics | | | |
|---|---|---|---|---|
| | Eddy Diffusion ($cm^2\ s^{-1}$) | Density[a] ($cm^{-3}$) | Pressure (bar) | Reference |
| Neptune | $\sim 3 \times 10^7$ | $\sim 3 \times 10^{11}$ | $\sim 10^{-8}$ | Broadfoot et al. 1989 |
| Uranus | $10^4$ | $1.1 \times 10^{15}$ | $2 \times 10^{-5}$ | Atreya et al. 1986; Herbert et al. 1987 |
| Saturn | $1.7(+4.3, -1.0) \times 10^8$<br>$8.0(+4.0, -4.0) \times 10^7$ | $1.2 \times 10^{11}$ | $4 \times 10^{-9}$ | Atreya 1982<br>Sandel et al. 1982 |
| Jupiter | $1.4(+0.8, -0.7) \times 10^6$ | $1.4 \times 10^{13}$ | $10^{-6}$ | Atreya et al. 1981; McConnell et al. 1981 |
| Titan | $1.0(+2.0, -0.7) \times 10^8$ | $2.7 \times 10^{10}$ | $6 \times 10^{-10}$ | Smith et al. 1982 |
| Earth | $(0.3 - 1) \times 10^6$ | $10^{13}$ | $3 \times 10^{-7}$ | Hunten 1975 |
| Venus | $10^7$ | $7.5 \times 10^{11}$ | $2 \times 10^{-8}$ | Von Zahn et al. 1980 |
| Mars | $(1.3 - 4.4) \times 10^8$ | $10^{10}$ | $2 \times 10^{-10}$ | Nier and McElroy 1977 |

[a]Atmospheric densities at the homopause correspond to the central values of $K_h$.

lyacetylenes. Unlike Jupiter and Saturn, however, these hydrocarbon products condense at the low temperatures prevalent in the middle atmosphere. Contrary to the pre-Voyager notion that the atmosphere of Uranus is remarkably clear, it is found that the aerosols are widely and extensively distributed. Despite its photodestruction, methane remains stable in the atmosphere of Uranus. This is expected to be accomplished by the re-evaporation or pyrolysis of the condensed aerosols in the deep troposphere, followed by chemical recycling to methane and its convection to the upper troposphere. Although the sedimentation of the condensed particles is relatively rapid, the same cannot be said of the downward transport of the gases from the region of their production in the upper stratosphere to the region where they condense. The vertical mixing on Uranus is found to be the least efficient of any of the planetary atmospheres. The question of latitudinal/seasonal variations in the hydrocarbons and the atmospheric vertical mixing needs extensive investigation at all levels—observational, theoretical, as well as in the area of laboratory measurements. Whatever little observational evidence that is currently available, does, in fact, point to significant latitudinal variations of aeronomic properties. Critical information on the dynamics and the microphysics of the cloud/haze particles is currently unavailable. Pertinent laboratory data on certain vapor pressures, and chemical kinetics of photon and charged-particle induced chemistry, are also sorely needed. Although it might be a long time before another spacecraft visits Uranus, continued interpretation of existing observations and of new Earth-based observations, especially

in light of new (as yet unavailable) laboratory data, is expected to enhance our understanding of Uranus' atmosphere in particular, and the origin of the outer solar system atmospheres in general.

*Acknowledgments* Discussions with B. Conrath, M. Flasar, F. Herbert, J. Pollack and R. Yelle have been helpful in clarifying many of the points in this chapter. Critical comments by D. Hunten, J. Bergstralh, and another (anonymous) referee were particularly beneficial for presenting a balanced review of the topic. SKA and BRS acknowledge partial support received for this work from NASA's Solar System Exploration Division. PNR acknowledges support from the Resident Research Associateship program and a NASA contract at Goddard Space Flight Center.